Chem

CellPress

Article

Air-stable radical polycyclic aromatic hydrogen-bonded organic frameworks

Bai-Tong Liu,[1,2,3,4,5,13] Tao Li,[6,7,13] Sheng-Hao Gong,[1,8,13] Jia-Chuan Liu,[6] Ze-Yu Ruan,[6] Han Han,[2,3,4] Timothy Y.-Z. Li,[4] Yuanning Feng,[7] Rui Wang,[1] Li Gong,[9] Xieming Xu,[1] Rong Cao,[1,5] Ming-Liang Tong,[6,*] J. Fraser Stoddart,[2,3,4,10,11,12] and Tian-Fu Liu[1,5,14,*]

[1]State Key Laboratory of Structural Chemistry, Fujian Institute of Research on the Structure of Matter, Chinese Academy of Sciences, Fuzhou 350002, China
[2]Department of Chemistry, University of Hong Kong, Hong Kong SAR 999077, China
[3]Center for Regenerative Nanomedicine, Northwestern University, 303 East Superior Street, Chicago, IL 60611, USA
[4]Department of Chemistry, Northwestern University, 2145 Sheridan Road, Evanston, IL 60208, USA
[5]University of Chinese Academy of Sciences, Beijing 101408, China
[6]Key Laboratory of Bioinorganic and Synthetic Chemistry of Ministry of Education, School of Chemistry, IGCME, GBRCE for Functional Molecular Engineering, Sun Yat-Sen University, Guangzhou 510275, China
[7]Department of Chemistry and Biochemistry, University of Oklahoma, 101 Stephenson Parkway, Norman, OK 73019, USA
[8]College of Chemistry and Materials Science, Fujian Normal University, Fuzhou 350117, China
[9]Instrumental Analysis and Research Center, Sun Yat-Sen University, Guangzhou 510275, China
[10]Stoddart Institute of Molecular Science, Department of Chemistry, Zhejiang University, Hangzhou 310027, China
[11]ZJU-Hangzhou Global Scientific and Technological Innovation Center, Hangzhou 311215, China
[12]School of Chemistry, University of New South Wales, Sydney, NSW 2052, Australia
[13]These authors contributed equally
[14]Lead contact
*Correspondence: tongml@mail.sysu.edu.cn (M.-L.T.), tfliu@fjirsm.ac.cn (T.-F.L.)
https://doi.org/10.1016/j.chempr.2025.102445

THE BIGGER PICTURE In the past, the construction of radical materials has been limited to the complex design and prolonged synthesis of radical building blocks. In this research, by chance, we made a discovery that some polycyclic aromatic monomers, previously considered to be air-unstable radicals, can be oxidized to stable radical materials when incorporated into hydrogen-bonded organic frameworks (HOFs). The intrinsic porosity of HOFs facilitates the formation of radicals with high spin concentrations thorough interactions with redox agents. The stable radical state displays non-observed decomposition in air for months. The formation of radicals narrows the band gap, transforming HOFs from insulators into typical n-type semiconductors. This research not only presents a facile and low-cost method for constructing air-stable radical HOF materials but also highlights the pivotal role that reticular chemistry can play in advancing radical semiconductors.

SUMMARY

Air-stable radical materials have emerged as promising candidates for next-generation electronic materials. Traditionally, constructing radical materials has required the intricate design and prolonged synthesis of radical building blocks. Herein, we have discovered a group of polycyclic aromatic monomers, previously considered to be air-unstable radicals, that can be oxidized to air-stable radical materials according to a post-synthetic protocol when they are incorporated into solid porous hydrogen-bonded organic frameworks (HOFs). The inherent porosity and crystallinity of HOFs facilitate extensive interactions with redox agents, such as tetravalent cerium(IV). These radical HOF materials exhibit high radical concentrations with paramagnetic behavior equivalent to two monomers sharing an unpaired electron. The HOFs can maintain their radical nature under ambient conditions on account of spin delocalization along the [$\pi\cdots\pi$] stacked units. The radical formation transforms the HOFs from insulators to typical n-type semiconductors. This discovery opens up avenues for exploring stable radical materials with diverse applications.

INTRODUCTION

The Pauli exclusion principle[1] requires that electrons always be arranged in pairs in closed-shell systems. Under certain conditions, however, some systems can be transformed into their open-shell states, characterized by unpaired electrons known[2,3] as (free) radicals. On the one hand, highly reactive radicals, often associated with biotoxins,[4] cause aging and other health issues. On the other hand, if the radical components are utilized rationally for the construction of functional organic materials,[5,6] they can exhibit a range of unique properties distinct from those of their closed-shell counterparts, offering unparalleled promise in the fields of organic semiconductors,[7] magnetic materials,[8,9] quantum information technologies,[10,11] and biomedicine.[12]

The principal hurdle[13,14] in transitioning radical materials from the laboratory into real-world applications lies in their inherent instability. Since the first persistent organic radical, triphenylmethyl, was reported by Gomberg[15] in 1900, researchers have developed numerous strategies for stabilizing radicals. Rational molecular-structure design provides a pivotal approach to improving radical stability, involving techniques such as the introduction of bulky protecting groups,[16] the enhancement of spin delocalization,[17] and the creation of electron push-pull systems.[18] In addition, noncovalent interactions,[3,19] together with the introduction of mechanical bonds,[20] have proven to be effective for enhancing the stability of radicals when they are encapsulated and stabilized inside mechanically interlocked molecules[21] (MIMs). These strategies,[3] however, focus predominantly on the radical building blocks and are constrained by complex design and prolonged syntheses.

Previously reported radically doped materials[22] offer valuable insights into the design and synthesis of air-stable radicals. These materials have demonstrated the generation of a limited number of radicals in solid matrices[23] when exposed to stimuli such as light,[24] electricity,[25] and redox agents,[26] leading to the doping of radicals in closed-shell matrices. Although the radical concentrations in these materials are typically low,[27] they can be stabilized in solid matrices for extended periods. Electrocrystallization is a well-established technique[28] for constructing perylene cation radical salts. Although radical doping can enhance the electrical conductivity[29] of perylene, it comes at the expense of stability. Moreover, certain reported radicals have been modified or used as monomers in constructing porous framework materials[30,31] for different applications. In previous research,[32] we discovered a pyrene-based hydrogen-bonded organic framework[33,34] (HOF), called **PFC-1**,[35] that showed potential for a radical cationic state when attached to an electrode for cyclic voltammetry (CV) measurements. This electrochemical process, however, does not truly oxidize the entire HOF into radical material for subsequent research and application.

The synergy between chemical redox agents and porous reticular chemistry[36] could offer a solution to this conundrum. Herein, we identified **PFC-1** and other polycyclic aromatic HOFs as initial closed-shell materials. We utilized ceric(IV) ammonium nitrate (CAN) as a chemical oxidant because it is capable of penetrating the channels of **PFC-1** and undergoing fast reactions with its building blocks. The highly ordered crystalline structure of the **PFC-1** scaffolds facilitates spin delocalization among the pyrene units, resulting in a significant enhancement in radical stability even when exposed to air under ambient conditions for months. The presence of unpaired electrons was confirmed by electron paramagnetic resonance (EPR) spectroscopy. The concentration of radicals, which we determined by counting counterions after single-crystal X-ray diffraction (SC-XRD) analyses and magnetic measurements, revealed that two pyrene monomers share one unpaired electron. The open-shell electronic structure of the radical HOF results in a narrowed band gap and imparts paramagnetism and semiconducting properties,[37,38] including improved electrical conductivity and near-infrared (NIR) photothermal conversion capabilities. Furthermore, this strategy can be extended to other polycyclic aromatic HOFs, offering even more possibilities for the construction of air-stable radical materials.

RESULTS AND DISCUSSION

Synthesis and structure of radical HOFs

1,3,6,8-Tetrakis(benzoic acid)pyrene (TBAPy) was synthesized via Suzuki coupling. Single crystals of **PFC-1** (Figures S1–S5) were obtained from a solution of TBAPy in *N*,*N*-dimethylacetamide/1,2,4-trichlorobenzene at 100°C. PFC-1 crystals were dispersed in acetonitrile (MeCN) and then mixed with a CAN solution in MeCN. Oxidation resulted in an immediate change in the mixture's color from yellow to green, accompanied by notable fluorescence quenching. These transformations are indicative of the formation of **PFC-1** in a radical state (**PFC-1-R**). This oxidation, however, could not be replicated in a TBAPy solution, signifying that the ordered solid state is a pivotal factor in generating and stabilizing the radicals (Figures 1, S6, and S7; Videos S1, S2, S3, S4, and S5). In contrast to the crystalline porous HOF, amorphous and nonporous TBAPy particles exhibited reduced reactivity toward CAN such that radicals occurred only on the particle surfaces and could be decomposed readily during solvent washing (Figure S8).

Despite rapid reaction kinetics, oxidation did not disrupt the crystalline structure, as demonstrated by consistent powder X-ray diffraction (PXRD) patterns (Figure 2A). More strikingly, the process underwent a structural transformation—as evidenced by SC-XRD investigations—in which radical formation did not induce significant alterations in bond lengths or angles. The distance between adjacent pyrene units increased slightly (from 3.77 to 3.79 Å; Figures S9 and S10; Table S1) because spin delocalization occurred parallel to the [$\pi\cdots\pi$]-stacked pyrene units.

Therefore, we can conclude that the color change (Figure 2B) and fluorescence quenching are not attributable to a shift in the molecular packing mode but are the result of changes in the electronic structure of **PFC-1**. A distinct single peak[39] (*g*-factor = 2.003) was observed in the EPR spectrum of **PFC-1-R**, confirming the presence of unpaired electrons. Temperature-dependent EPR measurements, conducted on **PFC-1-R** over a temperature range of 100–300 K, revealed[40] a decrease (Figure 2C) in peak-to-peak intensity as the temperature increased. Additional evidence for the existence of radicals was obtained from the ^{1}H NMR spectrum (Figure S2) of **PFC-1-R** recorded in CD_3SOCD_3. Although most radicals were quenched upon dissolution, the residual radicals in solution still resulted in noticeable peak broadening[41] for the aromatic protons in the ^{1}H NMR spectrum.

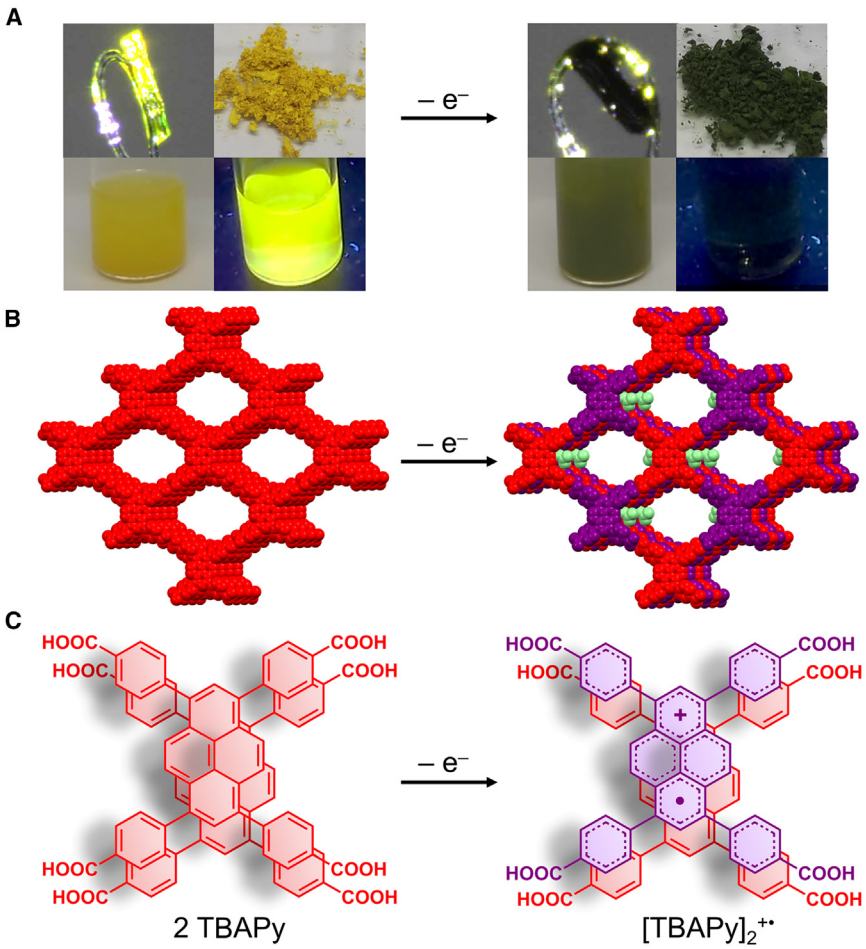

Figure 1. Radical formation

(A) Optical and fluorescent images of **PFC-1** (left) and **PFC-1-R** (right) in single-crystal, powder, and suspension states.

(B) Molecular packing of **PFC-1** (left) and **PFC-1-R** (right) according to the SC-XRD data. The green balls represent the NO_3^- counterions.

(C) Structural formulas of two TBAPy monomers in **PFC-1** and $[TBAPy]_2^{+\bullet}$ (two TBAPy molecules share one radical cation) in **PFC-1-R**.

The oxidation by CAN led to the loss of electrons from **PFC-1**, necessitating the presence of counterions to maintain charge conservation within the cationic radical framework. The counting of counterions not only allowed us to complete the reaction equations but also quantified the radical concentration within the HOF structures. The counterions were unfortunately highly disordered in the pores of the framework, and no satisfactory disordered model could be obtained according to the SC-XRD data. Some evidence comes from the characteristic peaks for NO_3^- observed by X-ray photoelectron spectroscopy (XPS) and in Fourier-transformed infrared (FT-IR) spectra (Figures S13 and S14). In order to quantify the NO_3^- content accurately in **PFC-1-R**, we employed ion chromatography (IC),[42] which revealed a ratio of approximately 2:1 between TBAPy and NO_3^- (see Figure S15). These results support the conclusion that two TBAPy molecules share one unpaired electron in the crystal structure. The oxidation leading to radical formation can be described by the following balanced equation:

$$2\ \mathrm{TBAPy} + (NH_4)_2 \cdot [Ce(NO_3)_6] = [\mathrm{TBAPy}]_2^{+\bullet} \cdot NO_3^- + Ce(NO_3)_3 + 2\ NH_4NO_3$$

Furthermore, the presence of counterions caused a reduction in the gas-adsorption capacity of N_2 and CO_2, as well as a decrease in the Brunauer-Emmett-Teller (BET) surface area (see Figures 2D, 2E, S11, and S12).

The formation of radicals in **PFC-1** resulted in significant fluorescence quenching, as evidenced by a comparison of photoluminescence spectra, lifetime decay profiles, and quantum yields (see Equation S1 and Figures S16–S18). This fluorescence-quenching phenomenon serves as an indicator of conducting a redox titration. According to the titration curve, the ideal reaction equivalent of [CAN]:[TBAPy] should be 1:2. We dispersed nanosized **PFC-1** in MeCN at an extremely dilute concentration (10 μM) to create an approximately homogenous system, whereas we injected CAN in MeCN solution (1,000 μM) in aliquots. We used photoluminescence spectra to monitor fluorescence quenching. Kinetic traces (Figure 2F) were generated on the basis of the normalized emission intensity at 533 nm. During the initial stages of the titration, a linear correlation was observed between the fluorescence intensity and the concentration of CAN. As the titration progressed, this dynamic response saturated gradually and ultimately reached a stoichiometry of 1:2 for [CAN]:[TBAPy].

We investigated the electrochromic properties of **PFC-1** in detail in order to confirm the cationic nature of **PFC-1-R**. CV measurements conducted at slow scanning rates of 0.01 V/s led an oxidation band to appear at 1.0 V and reach its maximum intensity at 1.4 V, indicating an oxidation state of **PFC-1** (see Figure S19). Upon continuous charging at 1.4 V for 20 min, the color of the **PFC-1** thin film affixed to the electrode interface changed gradually from yellow to green (see Video S6). Furthermore, the noticeable reversal in the Zeta potential from –9.3 to +14 mV and the enhancement of hydrophilicity reflected in a reduced static water contact angle (Figures S21 and S22) corroborate the inversion of surface charges.

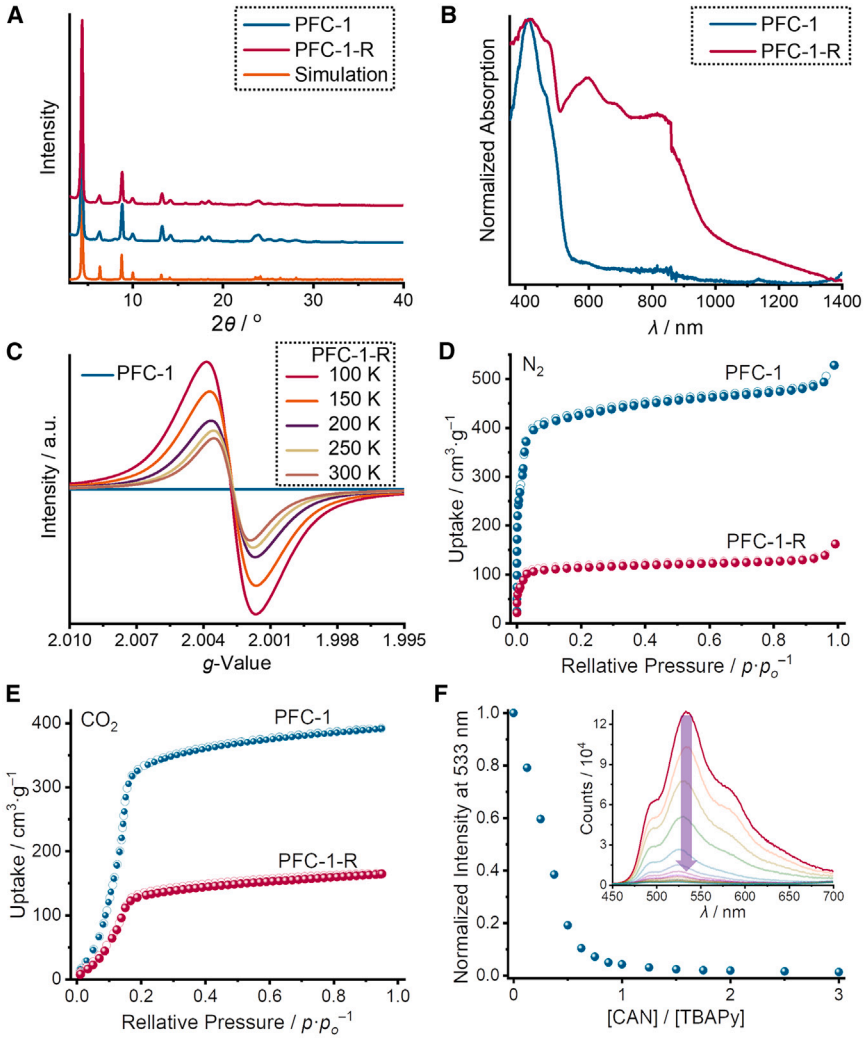

Figure 2. Structural characterization

(A–C) PXRD patterns (A), UV-vis-NIR absorbance spectra (B), and temperature-dependent EPR spectra (C) of **PRC-1** and **PFC-1-R**.

(D and E) N_2 isotherms at 77 K (D) and CO_2 isotherms at 195 K (E) of **PRC-1** and **PFC-1-R**.

(F) Changes in the fluorescence intensity monitored at 533 nm during titration with CAN. Inset: evolution of photoluminescence spectra of **PFC-1** suspension excited by a 375-nm laser during the titration.

Narrowed band gap and distinct properties

In contrast to the closed-shell **PFC-1**, radical formation resulted in a significant reduction in the band gap from 2.42 to 1.30 eV. The narrowed band gap became apparent through macroscopic alterations in color. **PFC-1-R** displayed a broad absorption band, spanning from 550 to 1,400 nm, as confirmed by solid ultraviolet-visible-NIR (UV-vis-NIR) absorbance spectra (Figure 2B) and diffuse reflectance spectroscopy (DRS). We determined the conduction-band potential (E_C) and valence-band potential (E_V) for both **PFC-1** and **PFC-1-R** by a combination of DRS spectra by using a Tauc plot and Mott-Schottky plots (see Figures 3A and 3B). The formation of radicals raised the E_V value from –1.06 eV for **PFC-1** to +0.24 eV for **PFC-1-R**, whereas it barely altered the E_C value. The semiconducting nature of **PFC-1-R** was verified by Hall effect measurements, which revealed a high charge-carrier density of 5.54×10^{16} cm^{-3}, high Hall electron mobility up to 2.17 $cm^2 \cdot V^{-1} \cdot s^{-1}$, and a negative Hall coefficient of –13.6 cm^3/C (see Table S3). Both the Mott-Schottky plots and the Hall effect measurements indicate that the charge carriers in **PFC-1-R** consist primarily of electrons, aligning **PFC-1-R** with the typical characteristics of n-type semiconductors.

The narrowed band gap of **PFC-1-R** resulted in enhanced absorption in the NIR region, an observation that contributes to its potential NIR photothermal conversion. When powdery **PFC-1-R** was deposited on a piece of quartz glass and exposed to 808 nm light at an intensity of 0.5 $W \cdot cm^{-2}$, its temperature rose rapidly from 25°C to 100°C within 30 s (Figure 3C). In contrast, **PFC-1** powders exhibited a minimal photothermal response under the same conditions. Nano-sized **PFC-1-R** was dispersed in MeCN as a suspension, and we monitored the temperature changes by using an infrared thermal imager to accurately determine the photothermal conversion efficiency (η). Under irradiation (808 nm/2 $W \cdot cm^{-2}$/0.5 cm^2), the temperature increased gradually until it reached a maximum of 44°C within 16 min and then gradually decreased over 50 min after the light had been turned off (Figure S24). The η value of **PFC-1-R** was calculated to be 24.6% (Equation S2–S5) according to a previously established method.[43,44]

The presence of unpaired electrons in **PFC-1-R**, coupled with its narrowed band gap,[45,46] contributes to its improved electrical conductivity. In order to quantify the enhanced conductivity, we compacted powdery **PFC-1** and **PFC-1-R** into thin circular discs. We constructed electrodes by connecting silver paste and gold bonding wire to both sides of the discs, forming a circuit. We obtained linear current-voltage (I-V) profiles by using a two-probe strategy (Figures 3D and S20), which indicated Ohmic contact. According to established practice (Equation S6), the conductivity of **PFC-1-R** was calculated to be 1.1×10^{-4} S cm^{-1}. This conductivity value is six orders of magnitude higher than that (1.5×10^{-10} S cm^{-1}) of the closed-shell **PFC-1** and is comparable to that of many classical semiconductors.[47,48] The significant improvement in electrical conductivity can be attributed to the spin delocalization in the radical state, which facilitates the electronic transfer among TBAPy building blocks.

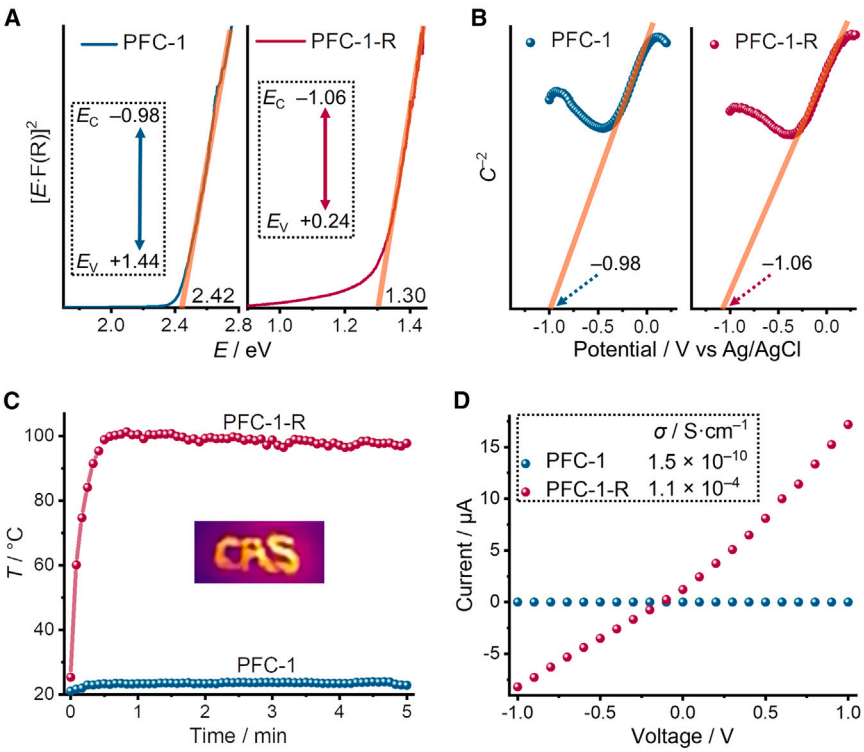

Figure 3. Narrowed band gap

(A and B) Tauc plot (A) and Mott-Schottky plots (B) of **PFC-1** and **PFC-1-R** for estimating the E_C and E_V values.

(C) Time course of the temperature rise of **PFC-1** and **PFC-1-R** powders on glass under NIR irradiation (808 nm, 0.5 W cm^{-2}).

(D) I-V curves of **PFC-1** and **PFC-1-R** discs.

Spin delocalization

Considering the anisotropy of the HOF crystals, investigating the relationship between crystal structures and anisotropic conductivities can contribute to determining the predominant direction of spin delocalization. We employed conducting atomic force microscopy (C-AFM) to measure the I-V curves[49] of a single crystal of **PFC-1-R** along different directions (Figure 4A). The size of the single crystal was determined by scanning electron microscopy (SEM). Notably, this rod-like single crystal exhibited substantially higher conductivity along its long axis than along its short axis. Crystal-face indexing based on the SC-XRD data (Figure 4B) confirmed that the TBAPy monomers are [π···π] stacked along the long axis and connected by hydrogen bonds forming 2D layers perpendicular to the long axis. This stacking arrangement is also supported by cryoelectron microscopy images of **PFC-1** reported in previous literature.[50,51] Combining these experimental results, we can conclude that the free electrons in **PFC-1-R** migrate preferentially along the [π···π]-stacked pyrene units in accordance with long-range spin delocalization.

We also conducted density functional theory (DFT) calculations by using the experimental crystallographic data for **PFC-1-R** to gain deeper insight into the microscopic details of spin delocalization. Figure 4C illustrates the isosurface of the spin density, which represents the distributions of an unpaired electron in two adjacent TBAPy monomers. The majority of unpaired electrons exhibit delocalization along the [π···π]-stacked direction such that they span both sides of the pyrene rings and localize on the eight boundary carbons in the pyrene structure. Furthermore, a smaller portion of unpaired electrons extends to the substituted benzoic acid functions. This significant spin delocalization leads to the dispersion of spin density and a reduction in reactivity, which is considered the primary factor contributing to the radical stabilization in **PFC-1-R**.

In order to investigate the magnetic properties of the stable radicals in **PFC-1-R**, we conducted a series of superconducting quantum interference device (SQUID) measurements. The molecular weight (M_w) of **PFC-1-R** was determined to be 1,427 g·mol^{-1} according to the formula of $[TBAPy]_2^{+\cdot}\cdot NO_3^-$. The temperature-dependent magnetization curve revealed a sharp increase in magnetic susceptibility (χ) with decreasing temperature (T), indicative of paramagnetism (Figure 5A). Furthermore, the $\chi{\cdot}T$-T plot reached a maximum value of approximately 0.375 $cm^3{\cdot}K{\cdot}mol^{-1}$ at 300 K (Figure 5B), consistent with a single-spin system.[52] The χ^{-1}-T plot was fitted linearly over the temperature range of 100–300 K in accordance with the Curie-Weiss law. The nonlinear deviations below 100 K (inset in Figure 5A) indicate a certain degree of antiferromagnetic interactions, which can be attributed to the influence of spin-spin coupling. At a fixed temperature of 2 K, the magnetization (M) displayed reversible changes with the applied magnetic field (H) (see Figure S25). Field-dependent magnetization was recorded at temperatures of 2, 3, 5, and 10 K. By using the scaling parameter ($H{\cdot}T^{-1}$) as the x coordinate, we fit all magnetization curves (Figure 5C) measured at different temperatures[53] in excellent fashion to a single Brillouin function with J = 1/2 (see Equation S7 and Figure S26). In addition, we employed magnetic force microscopy to visualize the surface magnetic distribution on a **PFC-1-R** single crystal (Figure S29), revealing the band-shaped magnetic interactions.

Radical stability and substrate extension

In order to assess the long-term radical stability of the **PFC-1-R**, we stored it in an EPR tube under an atmosphere of air. We monitored the EPR signals over time to track the radical decomposition process. Remarkably, **PFC-1-R** exhibited a slow attenuation of the EPR signals (Figure 5D), signifying its capability to remain stable in air for months. PFC-1-R also maintained high crystallinity even after being stored in air for 1 year (Figure S30). In contrast, when immersed in solvents, the radical state of **PFC-1-R** was quenched within 3 days in MeCN and within 1 day in water (see Figure S31). The exceptional radical stability of **PFC-1-R** expands its potential applications into real-life scenarios.

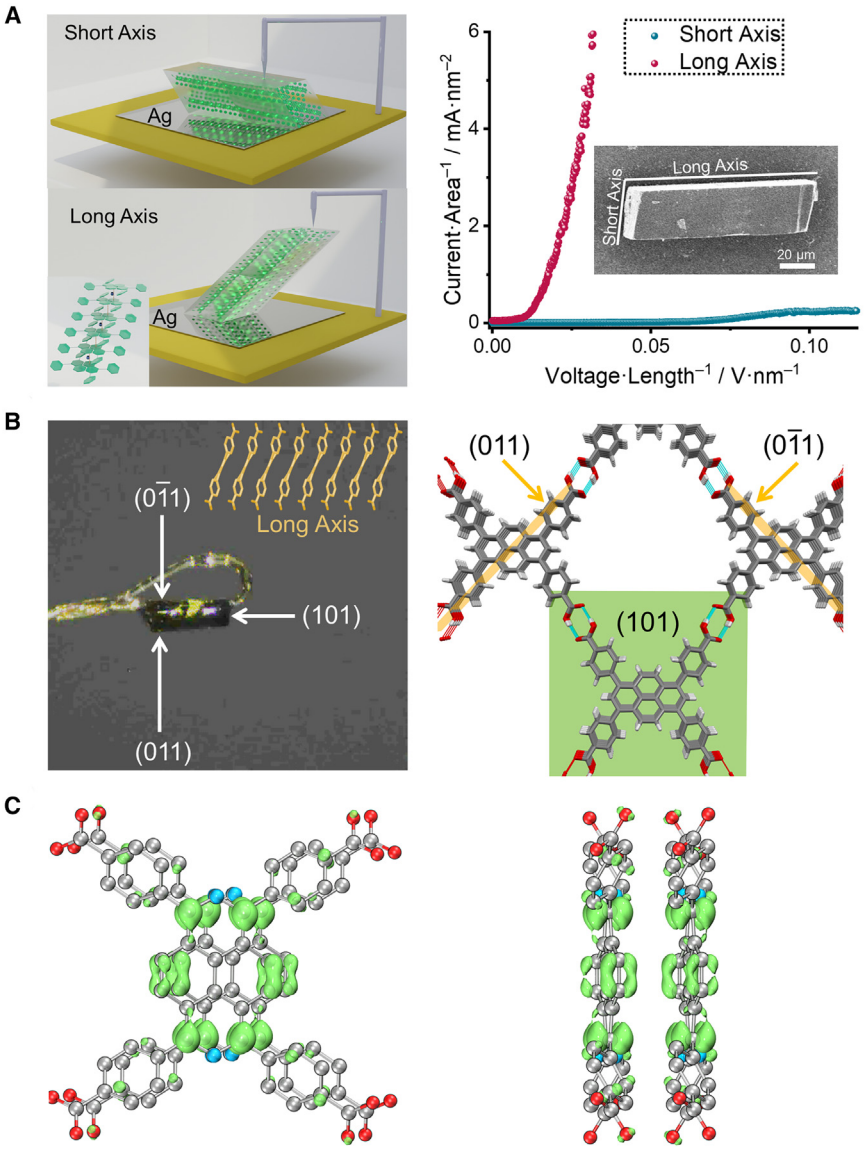

Figure 4. Spin delocalization

(A) Anisotropic electrical conductivity of a single crystal of **PFC-1-R** measured by C-AFM.

(B) Crystal-face indexing based on the SC-XRD data.

(C) Calculated spin density of two adjacent TBAPy monomers in **PFC-1-R** viewed along the *a* and *b* axes. The isosurface of the spin density is represented by an isovalue of 0.002 electrons·Å^{-3}. The green and blue isosurfaces indicate the α- and β-spin electrons, respectively.

We synthesized a series of polycyclic aromatic HOFs and subjected them to the same treatment with a CAN solution to investigate the applicability of this strategy. We observed that color changes and EPR signals also occurred in three HOFs composed of naphthoic-acid-substituted and ethynylbenzoic-acid-substituted pyrene, as well as in perylene monomers, but not in the non-substituted pyrene-based HOF (see Figures S32–S36). This result indicates that the substitutions on the monomers also play a critical role in spin delocalization and are necessary for radical stabilization in this HOF series.

The combination of air-stable radicals and porous HOFs opens up potential applications in energy conservation and biomedicine. The presence of stable radicals makes radical HOFs promising candidates for organic electrodes. Their tunable electronic properties and high surface area can enhance charge storage and ion transport. With appropriate functionalization, radical HOFs could be tailored for applications in drug delivery, particularly for therapies requiring redox-active environments. In addition, the radical HOFs can be synthesized under mild conditions, reducing the energy and cost barriers for large-scale production.

Conclusions

We have introduced a facile and effective strategy for the construction of air-stable radical HOFs through post-synthetic oxidation. Several key innovations can be highlighted. (1) The porous nature of the HOFs allows efficient permeation of oxidants into the channels, enabling adequate radical production. This process results in a high spin concentration where every two 1,3,6,8-tetrakis-(benzoic acid)pyrene monomers share one unpaired electron. (2) These distinctive radicals can be synthesized exclusively by solid-state reactions within HOFs, affording a novel perspective for fabricating unconventional radicals inaccessible through solution-based approaches. (3) The extension of spin delocalization over the conjugated backbone contributes to the longevity of the radicals, resulting in exceptional radical stability in air and different solvents. (4) The open-shell electronic structure imparts distinctive physicochemical properties to these materials, such as improved conductivity, NIR photothermal capacity, and paramagnetism. (5) This strategy demonstrates its applicability to other polycyclic aromatic HOFs, unveiling the potential for fabricating stable radical HOF materials with unprecedented properties. Overall, this research could contribute to the understanding and development of air-stable radical porous materials, holding significant promise for future research and practical applications.

METHODS

Synthesis of PFC-1-R

CAN (100 mg) was dissolved in MeCN (10 mL) to form a clear solution. When as-synthesized **PFC-1** powders (160 mg) were

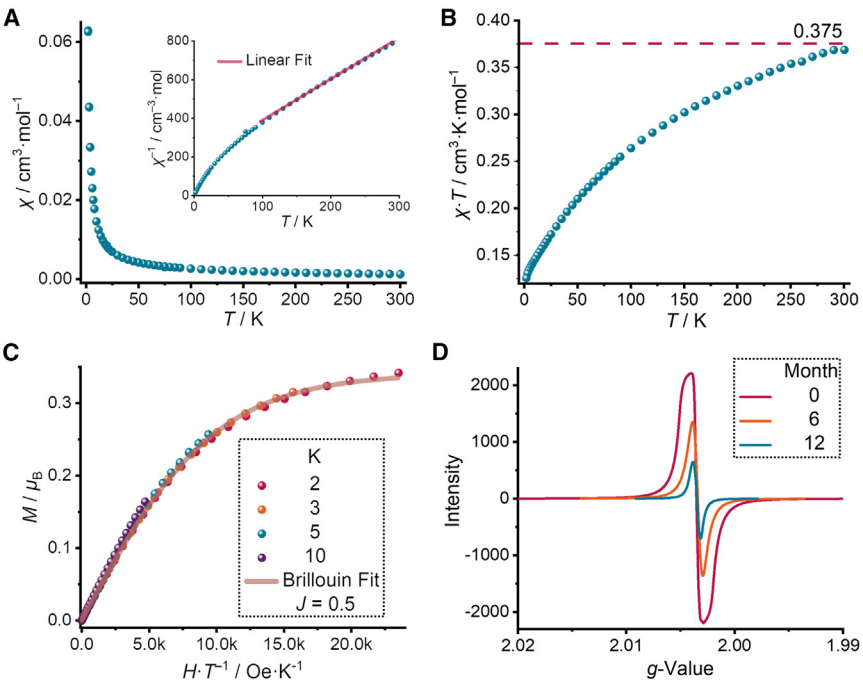

Figure 5. Magnetic measurements and radical air stability

(A) Temperature dependence of the magnetization of **PFC-1-R** ranging from 2 to 300 K obtained in an applied magnetic field of H = 10,000 Oe. Inset: linearly correlated region from 100 to 300 K in χ^{-1}-T plotting.

(B) $\chi \cdot T$-T plots. The horizontal dashed line $\chi \cdot T$ = 0.375 $cm^3 \cdot K$ indicates the theoretical value for an ideal paramagnetic radical.

(C) Magnetization as a function of $H \cdot T^{-1}$ at various temperatures, as well as a fitting curve according to the Brillouin function with J = 1/2 and g = 2.003.

(D) EPR spectra of **PFC-1-R** stored in air for different periods of time.

added to the above solution, the color of **PFC-1** changed immediately from yellow to green. The mixture was kept at room temperature for 1 day. After being washed three times with MeCN and being dried under vacuum at room temperature, the green **PFC-1-R** was harvested. For more experimental details, refer to the supplemental information.

RESOURCE AVAILABILITY

Lead contact

Requests for further information and resources should be directed to and will be fulfilled by the lead contact, Tian-Fu Liu (tfliu@fjirsm.ac.cn).

Materials availability

All other data supporting the findings of this study are available from the article and the supplemental information or from the lead contact upon reasonable request.

Data and code availability

The X-ray crystallographic data for **PFC-1-R** have been deposited at the Cambridge Crystallographic Data Centre (CCDC) under deposition number CCDC: 2215496. The data can be obtained free of charge from the CCDC via www.ccdc.cam.ac.uk. For more experimental details, please refer to the supplemental information.

ACKNOWLEDGMENTS

We gratefully acknowledge financial support from the Chinese Academy of Sciences (CAS) (JCTD-2022-12 to T.-F.L.), the CAS Youth Interdisciplinary Team, the National Natural Science Foundation of China (22071246 to T.-F.L.), and the Science Foundation of Fujian province (2024J010040 to T.-F.L.). We thank Rebecca Sponenburg at Northwestern University for the ion chromatography measurements, as well as Sun Yat-Sen University, the University of Hong Kong, and Northwestern University for supporting this research.

This work is dedicated to Professor Sir Fraser Stoddart, who was a towering figure in science, a dedicated mentor, and a dear friend to us all. His unparalleled contributions to chemistry and his unyielding support for his students and colleagues left an indelible mark on the field. We remember his dedication to assisting us in refining our manuscripts and sharing his insightful stories about science and life. His guiding principle of "people first, science second, money third," as steadfast as the Scottish Highlands, is also a compass for all of us in our careers.

This article also marks Dr. Bai-Tong Liu's (the first author of this work) and Timothy Li's first publication since joining Research Palace (RP) and Research Palace and Garden (RPG), which is a solemn reminder of the future research that we had planned out under Fraser's inspiration and will now pursue in his honor. Although he is no longer here to see these endeavors through, his legacy inspires us to push boundaries with the same boldness and brilliance that defined his career.

Fraser knew well the role of serendipitous discoveries in scientific research and embraced it with humor, grace, and an unyielding drive to persevere. Fraser's influence will live on through the research we undertake in the future. As we continue to build on the foundation he laid, may our ideas and collaborations be as enduring as his impact on science, "till a' the seas gang dry, my dear, and the rocks melt wi' the sun."

Gus am bris an latha, Fraser; you will be forever missed.

AUTHOR CONTRIBUTIONS

T.-F.L., J.F.S., and M.-L.T. guided the project. B.-T.L. designed and carried out most of the synthesis and characterization. T.L. conducted the EPR experiments. S.-H.G. assisted with the synthetic experiment. J.-C.L. conducted the DFT calculations. Z.-Y.R. conducted magnetic measurements. H.H. helped to perform the analysis of radical mechanism. Y.F. helped to perform the fluorescent titration. L.G. conducted the C-AFM measurements. X.X. carried out the electrical conductivity and Hall effect measurements. B.-T.L. finished the manuscript. T.Y.-Z.L. helped with English editing. T.-F.L., J.F.S., and M.-L.T. commented on and revised the manuscript.

DECLARATION OF INTERESTS

The authors declare no competing interests.

SUPPLEMENTAL INFORMATION

Supplemental information can be found online at https://doi.org/10.1016/j.chempr.2025.102445.

Received: June 25, 2024
Revised: November 26, 2024
Accepted: January 16, 2025
Published: February 12, 2025

REFERENCES

1. Massimi, M. (2005). Pauli's Exclusion Principle: The Origin and Validation of a Scientific Principle (Cambridge University Press).
2. Chen, Z.X., Li, Y., and Huang, F. (2021). Persistent and stable organic radicals: design, synthesis, and applications. Chem *7*, 288–332.
3. Tang, B., Zhao, J., Xu, J.-F., and Zhang, X. (2020). Tuning the stability of organic radicals: from covalent approaches to non-covalent approaches. Chem. Sci. *11*, 1192–1204.
4. Beckman, K.B., and Ames, B.N. (1998). The free radical theory of aging matures. Physiol. Rev. *78*, 547–581.
5. Ji, L., Shi, J., Wei, J., Yu, T., and Huang, W. (2020). Air-stable organic radicals: new-generation materials for flexible electronics? Adv. Mater. *32*, e1908015.
6. Shu, C., Yang, Z., and Rajca, A. (2023). From stable radicals to thermally robust high-spin diradicals and triradicals. Chem. Rev. *123*, 11954–12003.
7. Joo, Y., Agarkar, V., Sung, S.H., Savoie, B.M., and Boudouris, B.W. (2018). A nonconjugated radical polymer glass with high electrical conductivity. Science *359*, 1391–1395.
8. Phan, H., Herng, T.S., Wang, D., Li, X., Zeng, W., Ding, J., Loh, K.P., Shen Wee, A.T., and Wu, J. (2019). Room-temperature magnets based on 1,3,5-triazine-linked porous organic radical frameworks. Chem *5*, 1223–1234.
9. Jin, E., Asada, M., Xu, Q., Dalapati, S., Addicoat, M.A., Brady, M.A., Xu, H., Nakamura, T., Heine, T., Chen, Q., et al. (2017). Two-dimensional sp^2 carbon–conjugated covalent organic frameworks. Science *357*, 673–676.
10. Troiani, F., and Affronte, M. (2011). Molecular spins for quantum information technologies. Chem. Soc. Rev. *40*, 3119–3129.
11. Wasielewski, M.R., Forbes, M.D.E., Frank, N.L., Kowalski, K., Scholes, G.D., Yuen-Zhou, J., Baldo, M.A., Freedman, D.E., Goldsmith, R.H., Goodson, T., et al. (2020). Exploiting chemistry and molecular systems for quantum information science. Nat. Rev. Chem. *4*, 490–504.
12. Rivera, E.J., Sethi, R., Qu, F., Krishnamurthy, R., Muthupillai, R., et al. (2021). Nitroxide radicals@US-tubes: new spin labels for biomedical applications. Adv. Funct. Mater. *22*, 3691–3698.
13. Czapski, G., Holcman, J., and Bielski, B.H.J. (1994). Reactivity of nitric oxide with simple short-lived radicals in aqueous solutions. J. Am. Chem. Soc. *116*, 11465–11469.
14. Dolbier, W.R. (1996). Structure, reactivity, and chemistry of fluoroalkyl radicals. Chem. Rev. *96*, 1557–1584.
15. Gomberg, M. (1900). An instance of trivalent carbon: triphenylmethyl. J. Am. Chem. Soc. *22*, 757–771.
16. Tian, Y., Uchida, K., Kurata, H., Hirao, Y., Nishiuchi, T., and Kubo, T. (2014). Design and synthesis of new stable fluorenyl-based radicals. J. Am. Chem. Soc. *136*, 12784–12793.
17. Han, H., Zhang, D., Zhu, Z., Wei, R., Xiao, X., Wang, X., Liu, Y., Ma, Y., and Zhao, D. (2021). Aromatic stacking mediated spin–spin coupling in cyclophane-assembled diradicals. J. Am. Chem. Soc. *143*, 17690–17700.
18. Kumar, Y., Kumar, S., Mandal, K., and Mukhopadhyay, P. (2018). Isolation of tetracyano-naphthalenediimide and its stable planar radical anion. Angew. Chem. Int. Ed. *57*, 16318–16322.
19. DeHaven, B.A., Goodlett, R.L., Sindt, A.J., Noll, N., De Vetta, M., Smith, M.D., Martin, C.R., González, L., and Shimizu, L.S. (2018). Enhancing the stability of photogenerated benzophenone triplet radical pairs through supramolecular assembly. J. Am. Chem. Soc. *140*, 13064–13070.
20. Bruns, C.J., and Stoddart, J.F. (2016). The Nature of the Mechanical Bond: from Molecules to Machines (John Wiley & Sons).
21. Li, H., Zhu, Z., Fahrenbach, A.C., Savoie, B.M., Ke, C., Barnes, J.C., Lei, J., Zhao, Y.L., Lilley, L.M., Marks, T.J., et al. (2013). Mechanical bond-induced radical stabilization. J. Am. Chem. Soc. *135*, 456–467.
22. Wang, S., Li, F., Easley, A.D., and Lutkenhaus, J.L. (2019). Real-time insight into the doping mechanism of redox-active organic radical polymers. Nat. Mater. *18*, 69–75.
23. Xie, Y., Zhang, K., Yamauchi, Y., Oyaizu, K., and Jia, Z. (2021). Nitroxide radical polymers for emerging plastic energy storage and organic electronics: fundamentals, materials, and applications. Mater. Horiz. *8*, 803–829.
24. Ma, Y.J., Hu, J.X., Han, S.D., Pan, J., Li, J.H., and Wang, G.M. (2020). Manipulating on/off single-molecule magnet behavior in a Dy(III)-based photochromic complex. J. Am. Chem. Soc. *142*, 2682–2689.
25. Sun, J., Wu, Y., Wang, Y., Liu, Z., Cheng, C., Hartlieb, K.J., Wasielewski, M.R., and Stoddart, J.F. (2015). An electrochromic tristable molecular switch. J. Am. Chem. Soc. *137*, 13484–13487.
26. Han, H., Huang, Y., Tang, C., Liu, Y., Krzyaniak, M.D., Song, B., Li, X., Wu, G., Wu, Y., Zhang, R., et al. (2023). Spin-frustrated trisradical trication of prismcage. J. Am. Chem. Soc. *145*, 18402–18413.
27. Wu, S., Li, M., Phan, H., Wang, D., Herng, T.S., Ding, J., Lu, Z., and Wu, J. (2018). Toward two-dimensional π-conjugated covalent organic radical frameworks. Angew. Chem. Int. Ed. *57*, 8007–8011.
28. Endres, H., Keller, H.J., Müller, B., and Schweitzer, D. (1985). Electrocrystallization and structures of perylene radical salts: hexaperylene perchlorate, $(C_{20}H_{12})_6{}^+ClO_4{}^-$, triperylene perchlorate, $(C_{20}H_{12})_3{}^+ClO_4{}^-$, and diperylene hexafluorophosphate-tetrahydrofuran (3/2), $(C_{20}H_{12})_2{}^+PF_6{}^-.2/3C_4H_8O$. Acta Crystallogr. C Cryst. Struct. Commun. *41*, 607–613.
29. Oyama, M., Nitta, Y., and Okazaki, S. (2001). Anion-controlled electrocrystallization of perylene cation radical salts. J. Electroanal. Chem. *511*, 88–93.
30. Mi, Z., Yang, P., Wang, R., Unruangsri, J., Yang, W., Wang, C., and Guo, J. (2019). Stable radical cation-containing covalent organic frameworks exhibiting remarkable structure-enhanced photothermal conversion. J. Am. Chem. Soc. *141*, 14433–14442.
31. Xu, F., Xu, H., Chen, X., Wu, D., Wu, Y., Liu, H., Gu, C., Fu, R., and Jiang, D. (2015). Radical covalent organic frameworks: a general strategy to immobilize open-accessible polyradicals for high-performance capacitive energy storage. Angew. Chem. Int. Ed. *54*, 6814–6818.
32. Feng, J.-F., Liu, T.-F., and Cao, R. (2020). An electrochromic hydrogen-bonded organic framework film. Angew. Chem. Int. Ed. *59*, 22392–22396.
33. Wang, B., Lin, R.-B., Zhang, Z., Xiang, S., and Chen, B. (2020). Hydrogen-bonded organic frameworks as a tunable platform for functional materials. J. Am. Chem. Soc. *142*, 14399–14416.
34. Hisaki, I., Xin, C., Takahashi, K., and Nakamura, T. (2019). Designing hydrogen-bonded organic frameworks (HOFs) with permanent porosity. Angew. Chem. Int. Ed. *58*, 11160–11170.
35. Yin, Q., Zhao, P., Sa, R.J., Chen, G.C., Lü, J., Liu, T.F., and Cao, R. (2018). An ultra-robust and crystalline redeemable hydrogen-bonded oganic framework for synergistic chemo-photodynamic therapy. Angew. Chem. Int. Ed. *57*, 7691–7696.
36. Yaghi, O.M. (2019). Reticular chemistry in all dimensions. ACS Cent. Sci. *5*, 1295–1300.
37. Sun, Z., Ye, Q., Chi, C., and Wu, J. (2012). Low band gap polycyclic hydrocarbons: from closed-shell near infrared dyes and semiconductors to open-shell radicals. Chem. Soc. Rev. *41*, 7857–7889.
38. Zhang, Y., Yan, Y.F., Mi, J.R., Wang, S.H., Wang, M.S., and Guo, G.C. (2023). Bottom-up photosynthesis of an air-stable radical semiconductor showing photoconductivity to full solar spectrum and X-ray. Adv. Sci. *10*, e2302978.
39. Kato, K., and Osuka, A. (2019). Platforms for stable carbon-centered radicals. Angew. Chem. Int. Ed. Engl. *58*, 8978–8986.
40. Sun, Z., Zeng, Z., and Wu, J. (2014). Zethrenes, extended *p*-quinodimethanes, and periacenes with a snglet biradical ground state. Acc. Chem. Res. *47*, 2582–2591.
41. Pell, A.J., Pintacuda, G., and Grey, C.P. (2019). Paramagnetic NMR in solution and the solid state. Prog. Nucl. Magn. Reson. Spectrosc. *111*, 1–271.
42. After immersion in water, the HOF reverts from its radical to its neutral state, and the counterions are released from the HOF pores into the

solution. Ion chromatography can be used for identifying and quantifying the counterions.

43. Liu, C., Zhang, S., Li, J., Wei, J., Müllen, K., and Yin, M. (2019). A water-soluble, NIR-absorbing quaterrylenediimide chromophore for photoacoustic imaging and efficient photothermal cancer therapy. Angew. Chem. Int. Ed. *58*, 1638–1642.
44. Liu, B.T., Pan, X.H., Zhang, D.Y., Wang, R., Chen, J.Y., Fang, H.R., and Liu, T.F. (2021). Construction of function-oriented core–shell nanostructures in hydrogen-bonded organic frameworks for near-infrared-responsive bacterial inhibition. Angew. Chem. Int. Ed. *60*, 25701–25707.
45. Kirlikovali, K.O., Goswami, S., Mian, M.R., Krzyaniak, M.D., Wasielewski, M.R., Hupp, J.T., Li, P., and Farha, O.K. (2022). An electrically conductive tetrathiafulvalene-based hydrogen-bonded organic framework. ACS Mater. Lett. *4*, 128–135.
46. Louie, S., Zhong, Y., Bao, S.T., Schaack, C., Montoya, A., Jin, Z., Orchanian, N.M., Liu, Y., Lei, W., Harrison, K., et al. (2023). Coaxially conductive organic wires through self-assembly. J. Am. Chem. Soc. *145*, 4940–4945.
47. Orgiu, E., George, J., Hutchison, J.A., Devaux, E., Dayen, J.F., Doudin, B., Stellacci, F., Genet, C., Schachenmayer, J., Genes, C., et al. (2015). Conductivity in organic semiconductors hybridized with the vacuum field. Nat. Mater. *14*, 1123–1129.
48. Shi, J., Zhang, J., Yang, L., Qu, M., Qi, D.C., and Zhang, K.H.L. (2021). Wide bandgap oxide semiconductors: from materials physics to optoelectronic devices. Adv. Mater. *33*, e2006230.
49. Although C-AFM is reliable for contrasting anisotropic conductivity, it is not good for precisely measuring the conductivity value.
50. Chen, G., Tong, L., Huang, S., Huang, S., Zhu, F., and Ouyang, G. (2022). Hydrogen-bonded organic framework biomimetic entrapment allowing non-native biocatalytic activity in enzyme. Nat. Commun. *13*, 4816.
51. Chen, G., Huang, S., Ma, X., He, R., and Ouyang, G. (2023). Encapsulating and stabilizing enzymes using hydrogen-bonded organic frameworks. Nat. Protoc. *18*, 2032–2050.
52. Albold, U., Bamberger, H., Hallmen, P.P., van Slageren, J., and Sarkar, B. (2019). Strong exchange couplings drastically slow down magnetization relaxation in an air-stable Cobalt(II)-radical single-molecule magnet (SMM). Angew. Chem. Int. Ed. *58*, 9802–9806.
53. We set the angular momentum quantum number (*J*) to three different values (1/2, 1, and 3/2) to achieve the Brillouin function fitting. The *N* value was used as a variable parameter in the fitting process. The results of the fitting revealed that when *J* was set to 1/2, 1, and 3/2, the corresponding *N* values were determined to be 0.34, 0.16, and 0.10, respectively.

Chem

Article

Air-stable radical polycyclic aromatic hydrogen-bonded organic frameworks

Graphical abstract

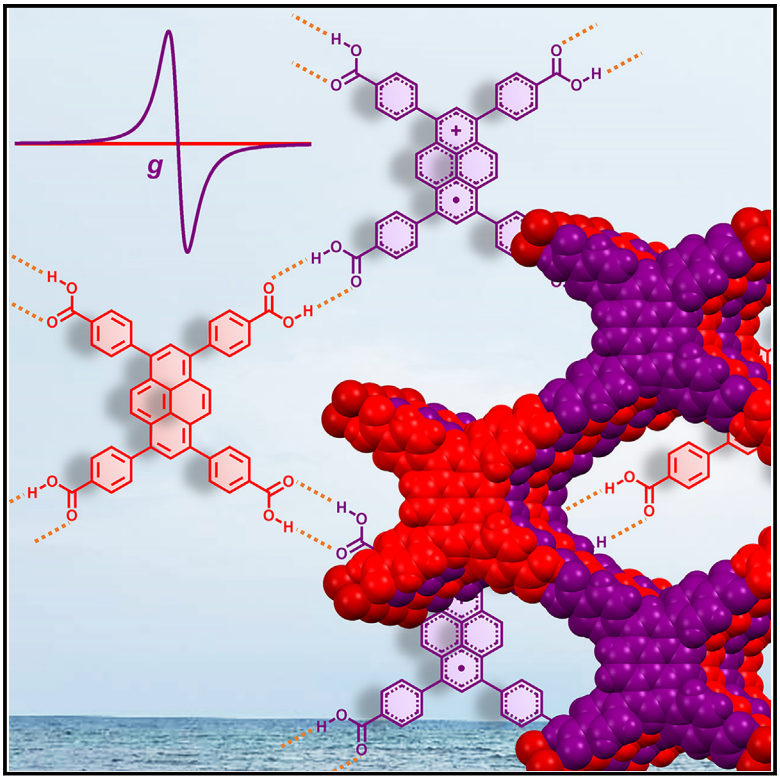

Highlights

- Air-stable radical porous HOFs have been synthesized
- Spin delocalization contributes to the stability of the radicals
- Radical HOFs show application prospects as organic semiconductors
- A series of polycyclic aromatic HOFs have the potential to form stable radicals

Authors

Bai-Tong Liu, Tao Li, Sheng-Hao Gong, ..., Ming-Liang Tong, J. Fraser Stoddart, Tian-Fu Liu

Correspondence

tongml@mail.sysu.edu.cn (M.-L.T.), tfliu@fjirsm.ac.cn (T.-F.L.)

In brief

Highly reactive radicals, commonly linked to biotoxins, are known to contribute to aging and various health complications. When these radical components are harnessed for the construction of functional organic materials, however, they can exhibit a diverse array of unique properties. Our research has unveiled that certain polycyclic aromatic porous materials possess the capability to undergo oxidation and thus yielding air-stable radicals. These radical materials hold immense potential in the fields of organic semiconductors, magnetic materials, quantum information technologies, and biomedicine.

Liu et al., 2025, Chem *11*, 102445
July 10, 2025
https://doi.org/10.1016/j.chempr.2025.102445

CellPress